NASA TECHNICAL NOTE

NASA TN D-1821

DYNAMIC RESPONSE OF RISING AND FALLING BALLOON WIND SENSORS WITH APPLICATION TO ESTIMATES OF WIND LOADS ON LAUNCH VEHICLES

by Wilmer H. Reed III Washington, NASA, Oct. 1963 refs

Langley Research Center
Langley Station, Hampton, Va.

NATIONAL AERONAUTICS AND SPACE ADMINISTRATION • WASHINGTON, D. C. • OCTOBER 1963

TECHNICAL NOTE D-1821

DYNAMIC RESPONSE OF RISING AND FALLING BALLOON WIND SENSORS WITH APPLICATION TO ESTIMATES OF WIND LOADS ON LAUNCH VEHICLES

By Wilmer H. Reed III

Langley Research Center
Langley Station, Hampton, Va.

NATIONAL AERONAUTICS AND SPACE ADMINISTRATION

NATIONAL AERONAUTICS AND SPACE ADMINISTRATION

TECHNICAL NOTE D-1821

DYNAMIC RESPONSE OF RISING AND FALLING BALLOON WIND SENSORS WITH APPLICATION TO ESTIMATES OF WIND LOADS ON LAUNCH VEHICLES

By Wilmer H. Reed III

SUMMARY

An analytical evaluation is made of the capabilities of balloon wind sensors to respond to detailed variations in the wind structure of the atmosphere, which can represent important load inputs for flexible launch vehicles. Both rising and falling spherical balloons are considered. It is found that for a balloon of given weight there is an optimum diameter for which the balloon response velocity is most sensitive to variations in the profile of horizontal winds. When the diameter of the balloon is larger than this optimum value the advantages of reducing the balloon weight to improve its dynamic response become relatively insignificant. The apparent mass of ambient air surrounding the balloon, which has often been neglected in previous investigations, is found to be of considerable importance at lower altitudes where launch vehicles often encounter maximum aerodynamic loads.

An approximate "desmoothing" procedure is developed which, under certain conditions, can be used to correct measured wind profiles for smoothing errors associated with inertia of the balloon wind sensor. Finally, an assessment is made of the reduction in the calculated elastic mode response of launch vehicles that results when the fine-grain structure of a wind input is smoothed by balloon inertia. These errors are evaluated for continuous random and triangular-shaped discrete gust inputs.

INTRODUCTION

Launch vehicles must survive a variety of load inputs during flight through the lower atmosphere. One of the most important of these inputs is the load due to wind velocities normal to the flight path of the vehicle.

By far the most abundant collection of wind-profile data upon which load estimates can be based has been obtained with the conventional AN/GMD-1 rawinsonde balloon sounding system. On the basis of a large sample of such data, various wind design criteria have been formulated, such as those given in references 1 to 4. Unfortunately, because of basic limitations in the GMD-1 wind measuring

system, these data give only a partial description of the actual wind environment. The detailed or fine-grain structure of the measured wind profile is to a large extent averaged out, both by inertia of the balloon and by the data-reduction procedures used to minimize the effects of random tracking errors.

Since the wind velocity fluctuations which are undetected by the conventional wind-measurement systems can represent a significant input to the elastic modes of a launch vehicle, considerable emphasis has been placed on the development of refined wind-sounding techniques. One such technique is the smoke-trail method described in reference 5. The method consists of measuring, by photographic triangulation, the horizontal wind velocities from a trail of smoke generated by a sounding rocket or launch vehicle. Another improved wind-sounding technique has been developed by the USAF Cambridge Research Laboratories (ref. 6) and the George C. Marshall Space Flight Center (ref. 7). This method involves tracking the ascent of a pressurized lightweight Mylar sphere with high-precision FPS-16 radar.

An indication of the importance of the fine-grain structure of wind profiles in the dynamic response of an elastic vehicle is given in references 5 and 8. These reports show comparisons of the responses calculated for the Scout vehicle by using as inputs a smoke-trail-measured wind profile and a simulated balloon-smoothing of the same profile. As might be expected, it was found that the dynamic bending-moment response determined for the detailed wind profile was significantly greater than that determined for the smoothed profile. These results represent two extreme conditions ranging from a highly detailed description of the wind input on the one hand to a grossly smoothed input on the other.

The following question might then be considered: If the elastic-mode response of a vertically rising launch vehicle is to be predicted on the basis of a balloon-measured wind profile, what mass, size, and terminal velocity should the balloon have in order to indicate sufficient details in the profile? Examination of this question represents the primary objective of the present paper. Specifically, the paper attempts to relate the wind-following capabilities of a rising or falling sphere to the dynamic aeroelastic response characteristics of a launch vehicle assumed to fly through the measured profile. Primary attention is given to the critical altitude interval wherein launch vehicles generally encounter maximum aerodynamic loads (20,000 to 45,000 feet).

Wind-measurement errors associated with the tracking system, data reduction procedures, and unsteady wake-induced motions of the balloon are not considered in the present treatment. The latter source of error was recently investigated by the NASA Langley Research Center and the U.S. Army Signal Corps in a large balloon hangar at the Lakehurst Naval Air Station. These studies showed that even under still air conditions spherical balloons follow an erratic path during ascent. The observed motion was characterized by horizontal fluctuation of the balloon trajectory about a mean vertical path. Wavelengths of the fluctuations were typically 10 to 20 balloon diameters; peak horizontal velocities were of the same order of magnitude as the ascent rate. Studies aimed at eliminating these wake-induced motions, by such methods as altering the balloon's surface features, are in progress. The present analysis treats one of the limitations on the accuracy of balloon-measured wind profiles, namely inertia effects. Other

factors, such as those previously mentioned will generally limit this accuracy still further, especially for the shorter wavelengths, but these effects are outside the scope of this report.

SYMBOLS

a_n	nth elastic-mode deflection of vehicle at reference station
a_{st}	static deflection
b	altitude increment of triangular gust
C_D	drag coefficient
D	diameter of sphere
D_y, D_z	drag in y- and z-direction, respectively
F_B	buoyant force
g	gravitational acceleration
H_b	frequency response of wind sensor
H_v	frequency response of vehicle
K_n	parameter defined by equation (26)
L	balloon lag distance
l	running-average length
M_n	generalized mass of mode n
m	structural mass of balloon or running mass of launch vehicle
m_a	apparent mass of ambient air associated with balloon
m_e	effective mass of balloon
m_g	mass of gas contained within balloon
P	generalized force per unit horizontal velocity
p	aerodynamic load distribution along vehicle length
s	Laplace operator
t	time

V_Z vertical velocity of launch vehicle

v_b horizontal component of balloon velocity

v_w horizontal component of wind velocity

$\overline{v_w}$ wind profile smoothed by a running-average operation

$v_{w,max}$ peak velocity of triangular-shaped gust

W weight of balloon

w_b vertical component of balloon velocity

$w_{b,t}$ terminal velocity of balloon

x distance along vehicle

y, z horizontal and vertical position coordinates

ζ_n equivalent viscous damping relative to critical damping for mode n

λ wind shear

μ mass-ratio parameter, $\frac{m_a}{m_g + m}$

ρ_a mass density of air

ρ_g density of gas contained in balloon

Φ power spectral density

$\phi_n(x)$ normalized shape of mode n

Ω_n space frequency associated with mode n, ω_n/V_Z

ω_n natural frequency of mode n

Dots over symbols indicate differentiation with respect to t; primes indicate differentiation with respect to z.

DYNAMIC RESPONSE OF BALLOON WIND SENSORS

Equations of Motion

Let $v_w(z)$ be the vertical profile of horizontal winds which, for convenience, is assumed to be planar and to remain fixed in space over the time

interval of interest. Let v_b and w_b be the horizontal and vertical velocity components of the sensor, which is here considered to be a rising or a falling spherical balloon. The equations of motion for the sensor are obtained by equating the external forces in the y- and the z-direction to the corresponding inertia forces:

(Horizontal inertia force) = (y drag component)

$$m_e \dot{v}_b = -D_y \tag{1a}$$

(Vertical inertia force) = (Gravity force) + (z drag component) + (Buoyant force)

$$m_e \dot{w}_b = -W - D_z + F_B \tag{1b}$$

The present analysis is restricted to consideration of wind inputs having wavelengths that are large relative to those associated with unsteady flow in the balloon wake. With this restriction it appears valid to assume that the aerodynamic force on the sensor is a pure drag-type force.

The various terms in equations (1a) and (1b) are now considered in more detail. The effective mass term comprises three parts:

$$m_e = m + m_a + m_g \tag{2}$$

where m is the structural mass of the body, m_a is the apparent mass of the ambient air affected by motions of the body, and m_g is the mass of the gas contained within the body. Here it has been assumed that the balloon and its contained gas move as a rigid body. For the special case of a spherical balloon the apparent mass is (see ref. 9)

$$m_a = \frac{1}{2} \rho_a \frac{\pi D^3}{6} \tag{3}$$

and the mass of the gas contained by the balloon is

$$m_g = \rho_g \frac{\pi D^3}{6} \tag{4}$$

When equations (3) and (4) are substituted into equation (2) the effective mass can be expressed as

$$m_e = \frac{W}{g} + \frac{\pi \rho_a D^3}{6} \left(\frac{1}{2} + \frac{\rho_g}{\rho_a} \right) \tag{5}$$

If an idealized condition is assumed wherein the pressure and temperature of the contained gas is the same as that of the ambient air, the following values of ρ_g/ρ_a are obtained:

For an air-filled balloon,

$$\rho_g/\rho_a = 1.0$$

For a helium-filled balloon,

$$\rho_g/\rho_a = 0.138$$

For a hydrogen-filled balloon,

$$\rho_g/\rho_a = 0.070$$

It should be noted that in the studies reported in references 6 and 10 the contribution of m_a to the total mass was considered negligible. This assumption is certainly justifiable at the high altitudes of interest in reference 10 (above 100,000 feet). However, in the altitude range for which typical launch vehicles experience maximum aerodynamic loads, this additional mass term is indeed significant. For example, at an altitude of 25,000 feet the 2-meter balloon considered in reference 6 has an apparent mass of 1,190 grams whereas the mass of the balloon structure is only 360 grams.

Other terms appearing in equations (1) and (2) are

Buoyant force:

$$F_B = \frac{\pi \rho_a g D^3}{6}\left(1 - \frac{\rho_g}{\rho_a}\right) \tag{6a}$$

The y component of drag:

$$D_y = \frac{\pi}{8}\rho_a C_D D^2 \left[(v_w - v_b)^2 + w_b^2\right] \frac{v_w - v_b}{\sqrt{(v_w - v_b)^2 + w_b^2}} \tag{6b}$$

The z component of drag:

$$D_z = \pm \frac{\pi}{8}\rho_a C_D D^2 \left[(v_w - v_b)^2 + w_b^2\right] \frac{w_b}{\sqrt{(v_w - v_b)^2 + w_b^2}} \tag{6c}$$

On the D_z term a positive sign is for ascent and negative sign for descent.

With the forces as defined in equations 6, the equations of motion are complicated by nonlinearities in v_b and w_b. If, however, it is assumed that accelerations in the vertical direction are negligible $\left(w_b \approx w_{b,t}\right)$ and that the horizontal-velocity errors $v_w - v_b$ are small in relation to the terminal

velocity $w_{b,t}$, considerable simplification can be achieved. Thus equations (1a) and (1b) become, respectively,

$$m_e\dot{v}_b + \left(\frac{\pi}{8}\rho_a C_D D^2 w_{b,t}\right)v_b = \left(\frac{\pi}{8}\rho_a C_D D^2 w_{b,t}\right)v_w(z) \tag{7}$$

and

$$w_{b,t} = \pm\sqrt{\left|\frac{4Dg\left(1 - \frac{\rho_g}{\rho_a}\right)}{3C_D} - \frac{8W}{\pi\rho_a C_D D^2}\right|} \tag{8}$$

where the positive sign is used when the terminal velocity is upward and the negative sign when it is downward.

Since the wind profile $v_w(z)$ is a function of altitude, it is convenient to use an altitude increment rather than time as the independent variable in equation (7). Thus, with the substitution

$$\dot{v}_b = \frac{dz}{dt}\frac{dv_b}{dz} = w_{b,t}v_b' \tag{9}$$

equation (7) reduces to simply

$$v_b' + \frac{1}{L}v_b = \frac{1}{L}v_w(z) \tag{10}$$

where the coefficient L is a characteristic length defined as

$$L = \frac{8m_e}{\pi\rho_a C_D D^2} \tag{11}$$

Interpretation of Balloon Response Equations

Physical significance of the parameter L.- Within the framework of the approximations used herein the dynamic properties of the wind sensor are completely specified by the single parameter L. This parameter, which is analogous to the time constant of a system, has some interesting and useful characteristics. For purposes of illustration consider the vertical profile of horizontal wind shown by the solid line in figure 1. The dashed line represents the horizontal velocity component of a falling body as it traverses such a profile. At an altitude z_0 the body is disturbed from equilibrium by a wind shear

$$\lambda_1 = \frac{v_{w,0} - v_{w,1}}{z_0 - z_1}\ \text{sec}^{-1} \tag{12}$$

The solution of equation (10) indicates that after the body has traveled a distance of about $3L$ beyond the disturbance, approximate steady-state equilibrium conditions are again established. The horizontal velocity of the body and the wind velocity are then related as follows: The velocity of the body at a given altitude is the same as the wind velocity it encountered a distance L prior to reaching that altitude, and the velocity error (the difference between the wind velocity and the body velocity) is simply

$$v_w - v_b = \pm\lambda L \tag{13}$$

where the sign on the right-hand side of equation (13) is positive for a rising body and negative for a falling body. Note also that abrupt variations in a profile, such as that indicated by the spike at altitude z_1 in figure 1, are smoothed by the inertia of the sensor. Thus, the parameter L may be considered a lag distance or memory length which related the instantaneous motion of the body to its previously encountered wind inputs.

In a subsequent section of the paper a "desmoothing" procedure will be illustrated whereby, if the lag length of the sensor is known, approximate

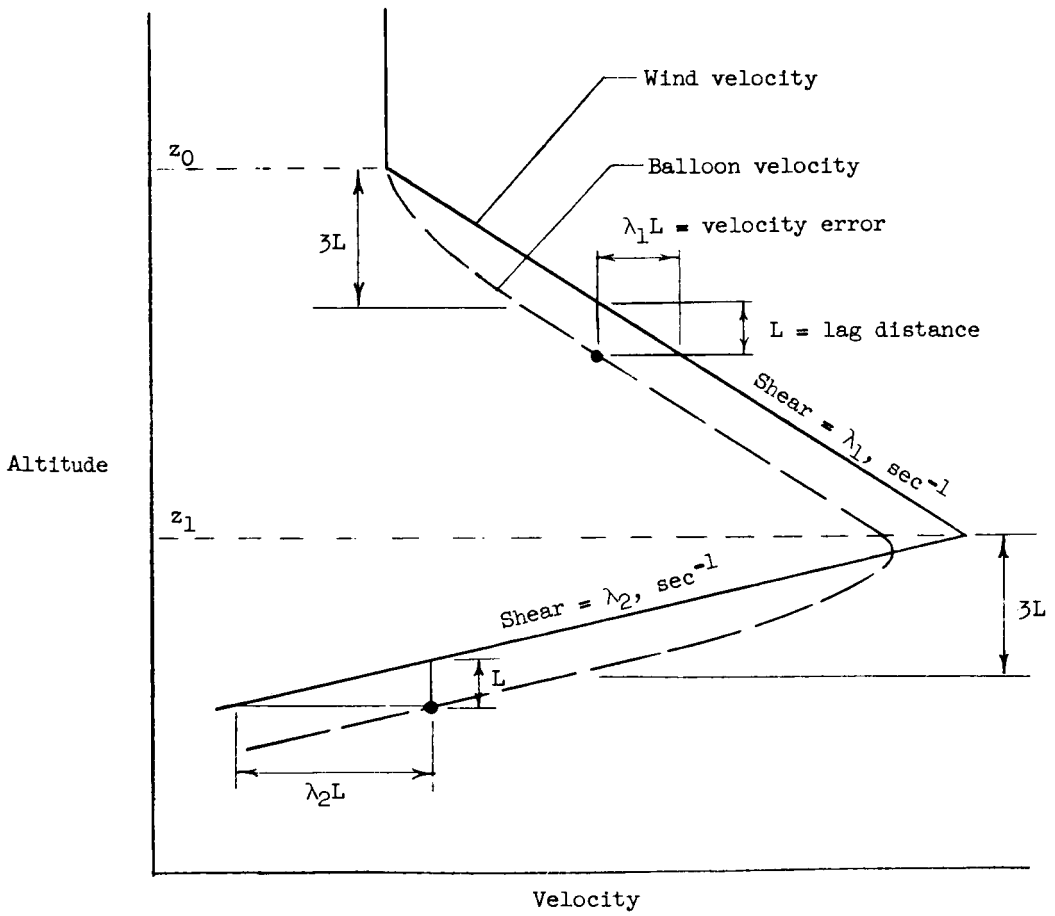

Figure 1.- Illustration of some properties of the balloon lag-distance parameter L.

corrections can be applied to the smoothing errors in a balloon-measured wind profile. It is therefore useful to express L in two alternate forms that embody the terminal velocity, which is a readily measurable quantity, and either ρ_a or C_D. Equations (5), (8), and (11) may be combined to eliminate either ρ_a or C_D. Thus, if it is assumed that C_D is known with more confidence than ρ_a, it would be desirable to determine L from the relationship for the first alternate form:

$$\left.\begin{aligned} L &= \frac{w_{b,t}^2}{g} + \frac{2D}{C_D} \qquad \text{(for rising spheres)} \\ L &= -\frac{w_{b,t}^2}{g} + \frac{2D}{C_D} \qquad \text{(for falling spheres)} \end{aligned}\right\} \tag{14}$$

If, on the other hand, ρ_a is known with better confidence, the second alternate form is used:

$$L = \frac{w_{b,t}^2}{g}\left|\frac{1 + \mu}{2\mu - 1}\right| \tag{15}$$

where μ is a mass-ratio parameter defined as

$$\mu = \frac{m_a}{m_g + m}$$

Comparison of several balloon wind sensors.- Equation (15) is shown graphically in figure 2(a) for rising spheres, and in figure 2(b) for falling spheres. Points which represent some existing balloon wind sensors are also plotted in figure 2 for an assumed altitude of 25,000 feet. The balloons considered are a rawinsonde weather balloon, a chaff-type pilot balloon, a 2-meter Mylar sphere (ref. 6), and a ROBIN falling sphere (ref. 11). The contained gas, which is assumed to be at ambient pressure, is hydrogen for the rising balloons and air for the falling balloons. The differences in performance between hydrogen-filled and helium-filled rising balloons are relatively small for the cases treated. Other pertinent physical properties for the balloons used in these calculations are presented in table I.

Note that for the rising balloons considered, the lag distance varies from a minimum of 10 feet for the chaff balloon to a maximum of 74 feet for the rawinsonde. The falling chaff balloon and the ROBIN have lag distances of 20 and 24 feet, respectively. As previously discussed, the wind-velocity errors associated with these lag distances can be evaluated in terms of wind shear by means of equation (13). These errors can be compared with the tracking errors of existing FPS-16 radar, which are estimated in reference 7 to have a maximum root-mean-square value of about 2.5 feet per second at altitudes where maximum winds normally occur.

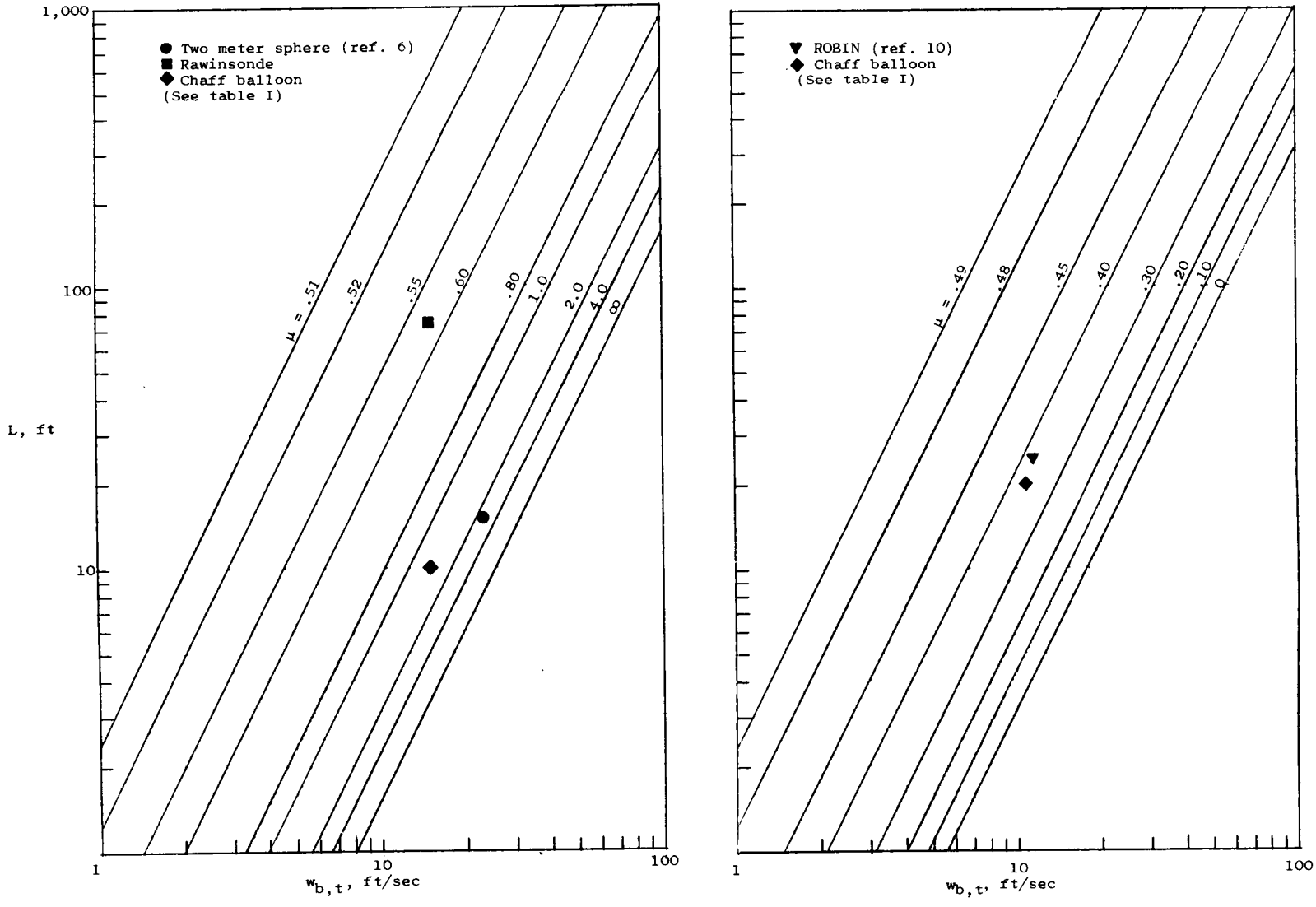

(a) Rising spheres.

(b) Falling spheres.

Figure 2.- The lag-distance parameter as a function of terminal velocity and mass ratio for rising and falling spherical bodies.

TABLE I.- PHYSICAL PROPERTIES OF BALLOONS CONSIDERED IN FIGURE 2

[Altitude = 25,000 feet]

Balloon type	Diam., ft	Weight		$w_{b,t}$, ft/sec	μ	L, ft
		lb	gm			
Hydrogen-filled rising balloons:						
2-meter balloon	6.57	0.77	360	23.0	2.300	15.0
Rawinsonde	7.50	6.20	2,810	15.0	0.573	74.2
Chaff balloon	3.90	0.33	150	15.3	1.35	10.1
Air-filled falling balloons:						
Chaff balloon	3.90	0.33	150	-10.6	0.380	20.1
Robin	3.28	0.25	115	-11.4	0.385	24.4

Optimum size-weight relations.- In this section it will be shown that for a balloon of given gross weight there is an optimum diameter for which the lag distance of the balloon has a minimum value.

Substituting equation (5) into equation (11) gives

$$C_D L = \frac{8W}{\pi \rho_a g D^2} + \frac{4D}{3}\left(\frac{1}{2} + \frac{\rho_g}{\rho_a}\right) \tag{16}$$

Consider the variation of $C_D L$ for an expansible balloon as it inflates. Equation (16) indicates that for the small diameters which exist at the start of inflation, the structural mass (given by the first term) predominates over the sum of the apparent air mass and the mass of contained gas (given by the second term), so that, for constant C_D, L decreases with $1/D^2$. As the balloon inflates further, however, the second term in equation (16) becomes predominant and L then increases with D. The diameter for which L has a minimum, or optimum, value for an assumed constant C_D can be determined by minimizing L in equation (16) with respect to D and thereby obtaining

$$D_{opt} = \left[\frac{12W}{g\pi\rho_a\left(\frac{1}{2} + \frac{\rho_g}{\rho_a}\right)}\right]^{1/3} \tag{17}$$

The L value associated with this optimum diameter is found to be

$$L_{opt} = \frac{1 + 2\frac{\rho_g}{\rho_a}}{C_D} D_{opt} \tag{18}$$

The volume of an expansible balloon changes with altitude in such a manner that $\rho_a D^3$ remains constant. As can be seen from equation (17) this also happens to be the manner in which the optimum diameter of a balloon varies with altitude. Thus, if the diameter of an expansible balloon is optimum at one altitude it will automatically change with altitude so as to remain optimum at all other altitudes for which C_D remains constant. In contrast, a fixed-diameter balloon, such as the 2-meter spherical balloon of reference 6, satisfies the optimum size-weight relations at only one altitude.

The variation of the quantity $C_D L$ with diameter for various balloon weights (eq. (16)) is shown in figure 3(a) for rising spheres and in figure 3(b) for

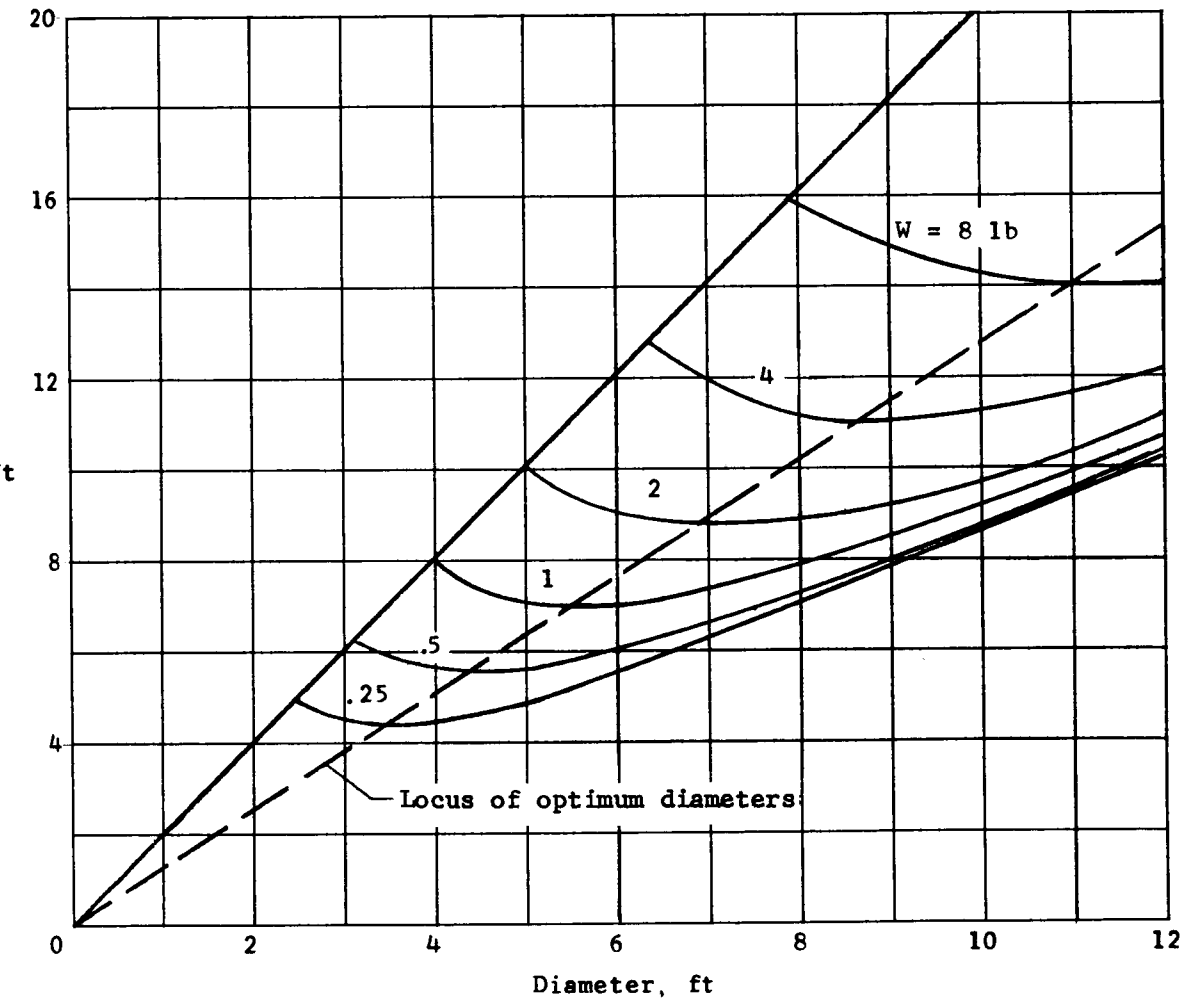

(a) Rising sphere. $\frac{\rho_g}{\rho_a} = 0.138$.

Figure 3.- The lag-distance parameter as a function of the weight and diameter of spherical bodies at an altitude of 25,000 feet.

falling spheres. It is assumed that the rising balloons contain helium $\left(\rho_g/\rho_a = 0.138\right)$ and the falling balloons contain air $\left(\rho_g/\rho_a = 1.0\right)$. The air density considered is $\rho_a = 0.00109$ slug/cubic foot, which corresponds to an altitude of 25,000 feet. The locus of optimum diameters is also shown in figures 3(a) and 3(b) by the dashed line that passes through the minimum point on each curve (see eq. (17)). The straight line along which the curves in figure 3(a) terminate represents the limiting condition of zero rate of climb for balloons at an altitude of 25,000 feet. This result is obtained by setting $w_{b,t}$ equal to 0 in equation (14), which gives $C_DL = 2D$. A point worth noting in figure 3 is that when the diameter of a balloon is large - large relative to its optimum value - the performance gains that can be realized by a reduction in structural weight become relatively insignificant.

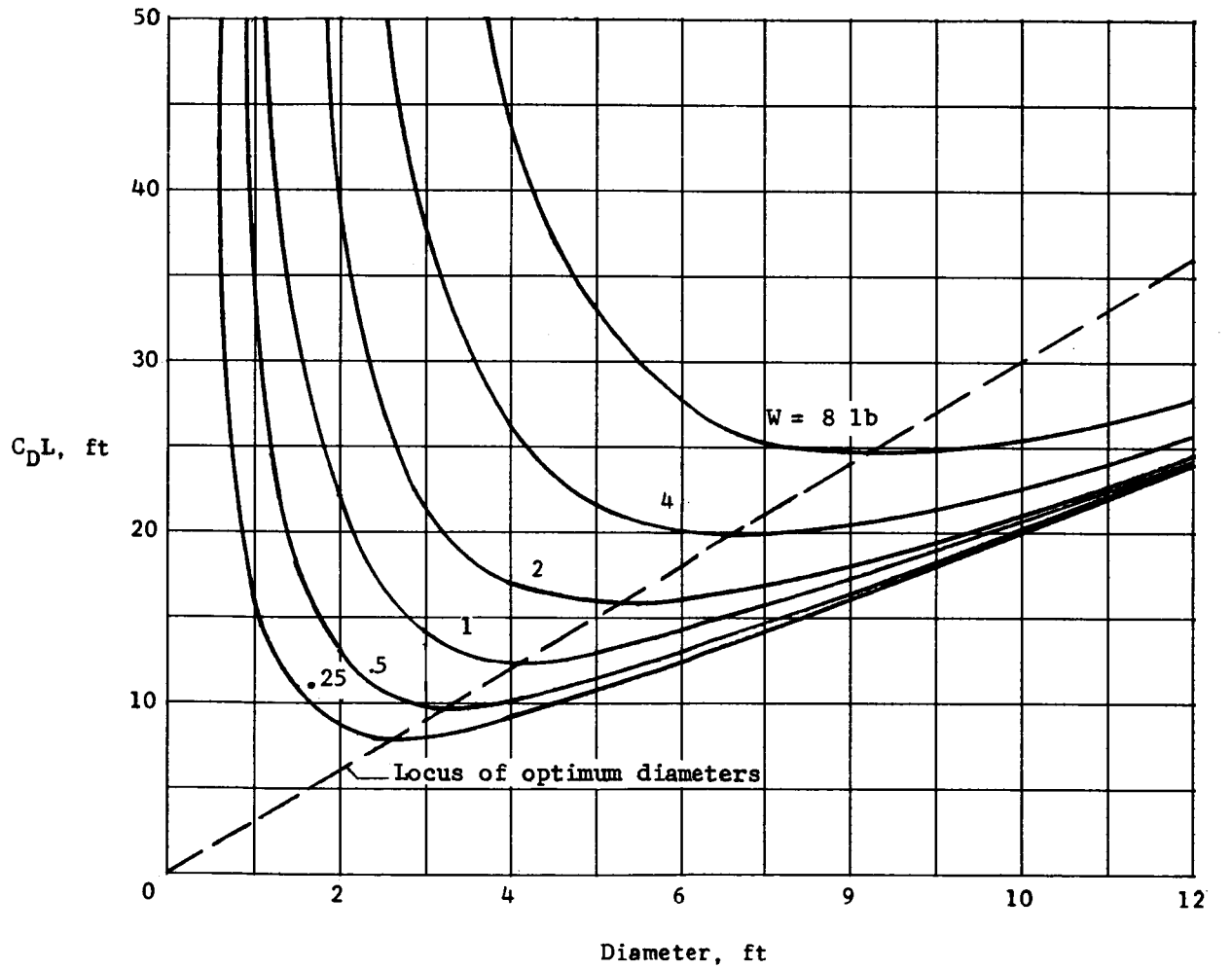

(b) Falling sphere. $\frac{\rho_g}{\rho_a} = 1.0$.

Figure 3.- Concluded.

Relation between L and a running-average distance.- In analytical investigations of vehicle response to detailed wind profiles measured by the smoke-trail technique, equivalent balloon-measured profiles have been simulated by smoothing the smoke-trail-measured profiles (see, for example, refs. 5 and 8). The smoothing technique often employed consists of simply averaging the velocities of the detailed profile over an interval extending an equal distance on each side of the altitude in question. It is of interest to determine the relation between this so-called "running average" length and the parameter L. An approximate equivalence between the lag length L and a running-average length l is found in the appendix to be

$$l \approx 3.46L \tag{19}$$

Thus, if tracking and data readout errors were not present, the equivalent running-average length for the rawinsonde balloon considered in table I would be approximately $l = 3.46 \times 74.2$ or 258 feet as contrasted with the 2,000 feet used in reference 8 to simulate the overall smoothing characteristics of the GMD-1 wind data.

Response of Falling Spheres to a Simulated Wind Profile

Analog-computer results.- For further insight into the wind-following characteristics of falling spheres, equations (1) have been solved on an analog computer by using a synthetic wind-profile input. In the simulation of this problem the buoyant force F_B was assumed to be zero, and the y and z components of drag were used in the nonlinear form given by equations (6). A constant drag coefficient of 0.1 was used in the analysis. This value may be considered a representative C_D for smooth spheres at Reynolds numbers above the critical value, which may vary from 2×10^5 to 5×10^5. Atmospheric density in the altitude range considered (20,000 to 30,000 feet) was assumed to vary according to the relation

$$\rho_a = 0.0034e^{-z/22,000} \text{ slug/cu ft} \tag{20}$$

where the altitude z is given in feet. The simulated wind profile through which the spheres are "dropped" had variations in wind shear ranging from $\lambda = 0$ to $\lambda = 0.10 \text{ sec}^{-1}$, as shown in figure 4.

In figure 4(a) the diameter of a 1.00-pound sphere is varied and in figure 4(b) the weight is varied for a 6-foot-diameter sphere. In both cases the bodies were assumed to be released from rest at an altitude of 30,000 feet. Figure 3(b) shows that the optimum diameter of a 1.00-pound falling sphere is approximately 4 feet. This fact is also evident in figure 4(a), where it can be seen that the 4-foot-diameter body follows the input more closely than either the 2- or the 8-foot-diameter body. Furthermore, the severe degradation in the velocity-tracking capability of a 1.00-pound sphere that is seen to occur in figure 4(a) when the diameter is reduced from 2 feet to 1 foot is also evidenced in figure 3(b) by the manner in which C_DL abruptly increases in this diameter

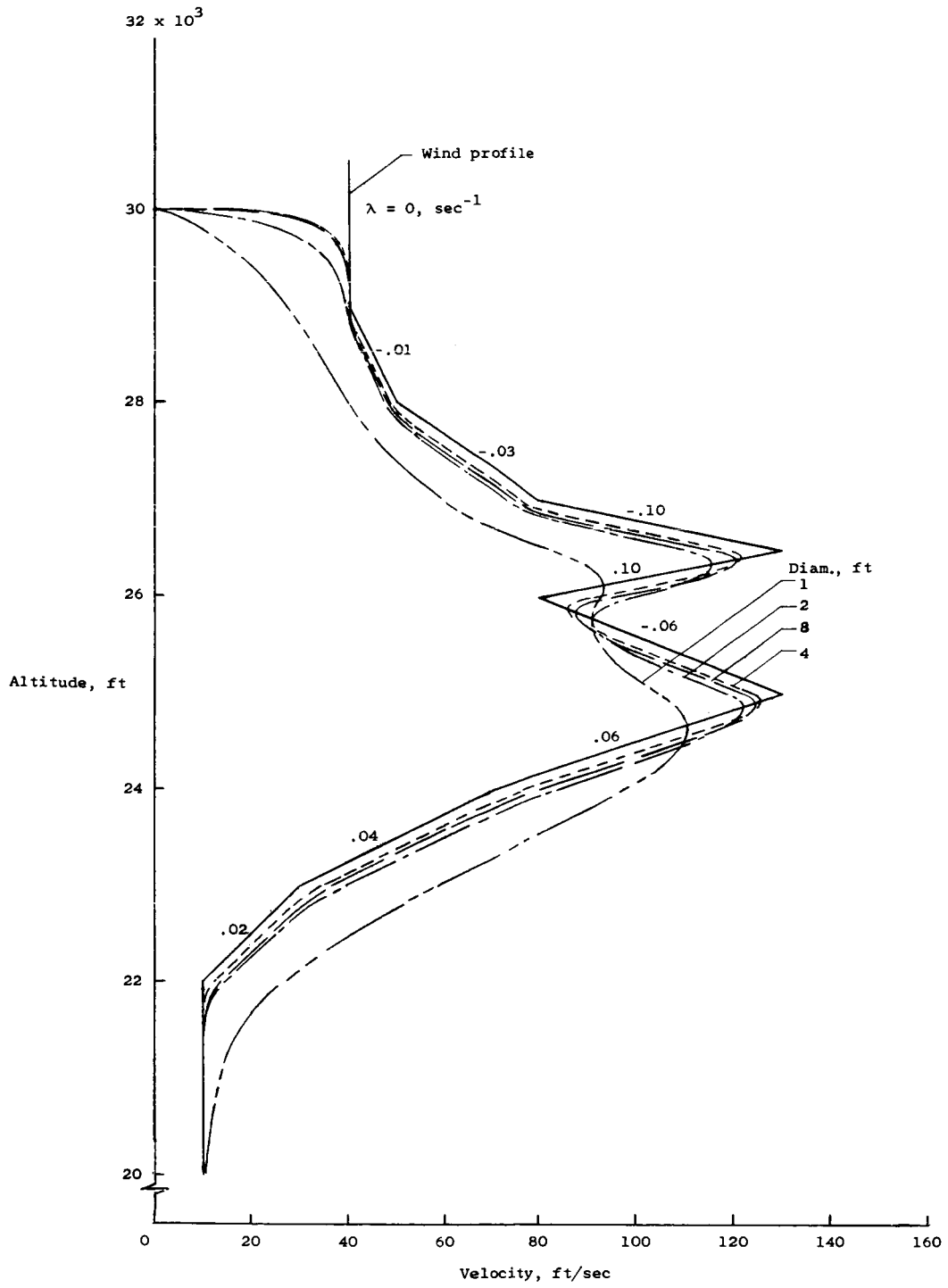

(a) Weight = 1.00 pound.

Figure 4.- Analog-computer solutions of the response of falling spheres to a simulated wind profile.

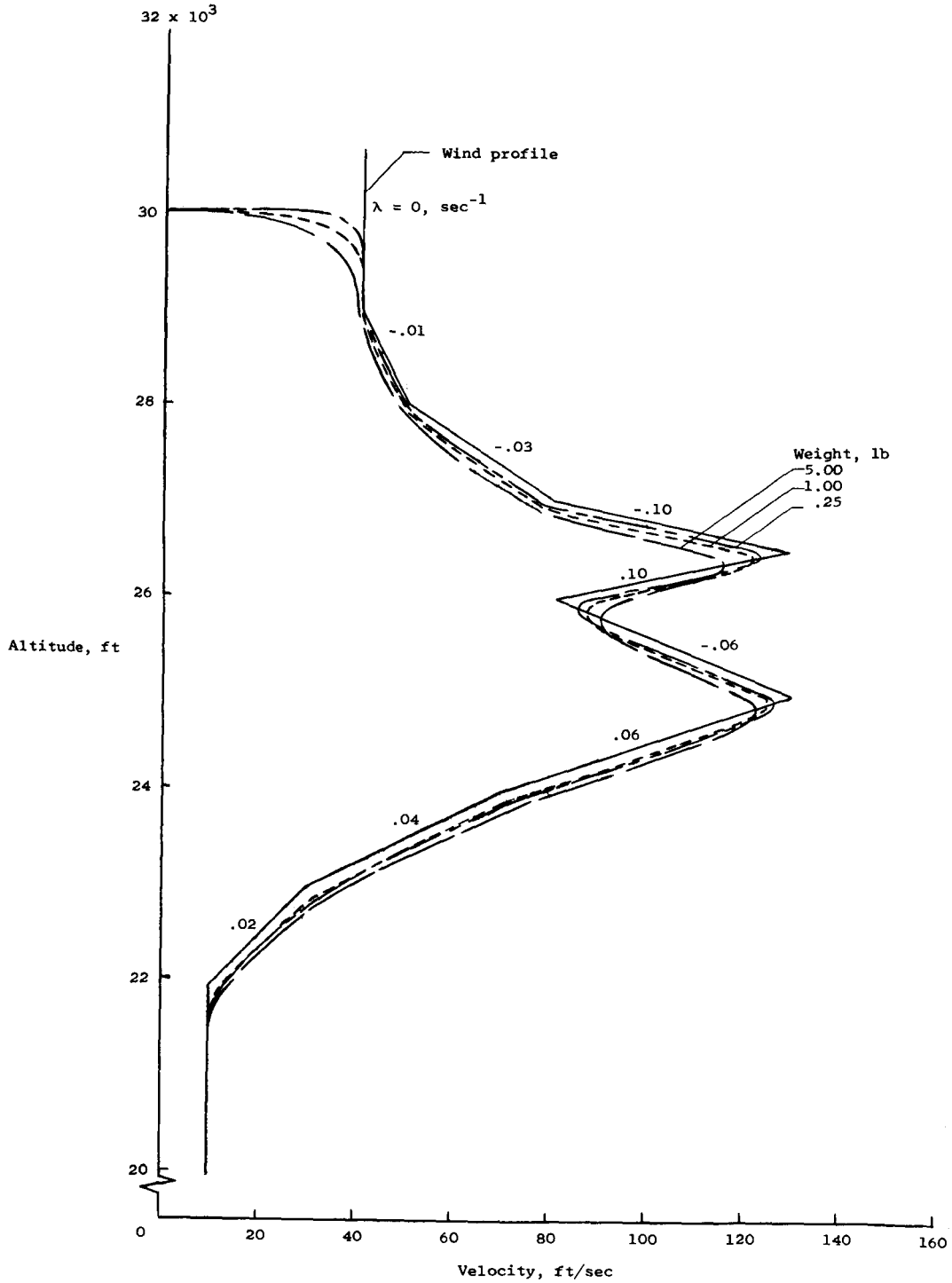

(b) Diameter = 6 feet.

Figure 4.- Concluded.

range. For the 6-foot-diameter sphere in figure 4(b) the difference between the responses of the 1.00-pound and the 0.25-pound sphere is indeed small. This fact confirms a previously mentioned point regarding the relatively insignificant gains that can be achieved through weight reductions when the balloon diameter is greater than an optimum value.

An approximate "desmoothing" procedure.- As illustrated by the plots in figure 4, the balloon response lags behind the wind-profile input and tends to smooth its detailed features. A possible method for correcting a measured wind profile for balloon-smoothing errors will now be considered. The basic assumption made is that the wind profile can be approximated by a series of straight-line segments of length 3L or greater. Application of the procedure for the case of the 1.00-pound 2-foot-diameter falling sphere of figure 4(a) is illustrated in figure 5. With reference to figure 5 the "desmoothing" procedure may be described as follows:

1. From equation (14) or (15) determine the variation of L with altitude. (See right-hand side of fig. 5.)

2. Represent the balloon velocity-response curve (A) with a series of straight-line segments. The altitude interval covered by each segment should be at least 3L, where L is the average balloon lag distance for that altitude interval.

3. Shift the straight-line segments (B) vertically a distance L in a direction opposite that traveled by the balloon. For the case of figure 5, a falling sphere, the curve is shifted upward. This curve (C) represents the corrected or "desmoothed" profile.

Comparison of the wind profile corrected for smoothing errors - curve C - with the true wind profile used as an input - curve D - shows that the agreement between the profiles is good everywhere except in the region of highest wind shear ($\lambda = \pm 0.10$ sec^{-1}; see fig. 4). In this region the two profiles differ because the wind shear changed before steady-state response conditions were established by the balloon, that is, before it traveled a distance 3L. Note that the desmoothed profile always indicates a triangular peak in the wind profile regardless of the actual shape of the peak.

It should be mentioned that at very high altitudes, falling bodies, such as ROBIN spheres (ref. 11), will have much larger L values than those considered here. Consequently, the steady-state response conditions required in the procedure may often not be obtained at these altitudes.

RESPONSE OF FLEXIBLE LAUNCH VEHICLES TO WIND PROFILES

Simplifying Assumptions

Previous sections of the paper have concerned the wind-tracking capabilities of a wind sensor with little consideration given to the accuracy requirements

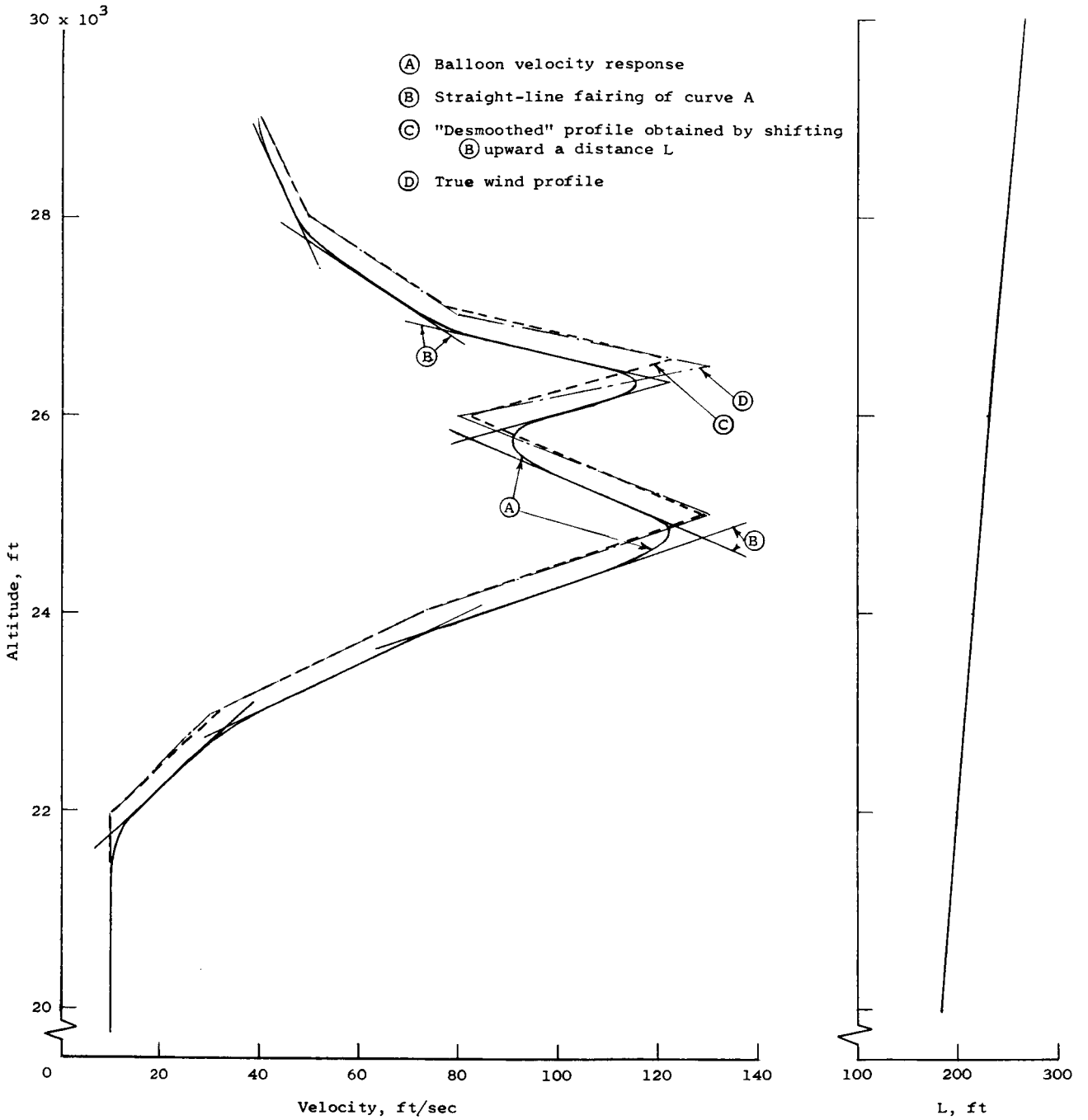

Figure 5.- Illustration of an approximate method of "desmoothing" a balloon-smoothed wind profile. Falling sphere; D = 2 feet; W = 1.00 pound.

in applying these measurements to launch-vehicle response problems. An attempt will now be made to interpret wind-measurement errors in terms of the vehicle response errors that will result when the smoothed wind profile instead of the detailed profile is used as the forcing function. Since the principal differences in response of a vehicle to these two forcing functions will occur in the elastic modes, only elastic modes will be considered herein. Furthermore, to avoid complications which would tend to obscure the basic results being sought, the following simplifying assumptions have been introduced:

1. The vehicle response is represented by a single-degree-of-freedom, constant-coefficient system.

2. The wind sensor and the vehicle are assumed to experience the same wind profile.

3. For the case of random wind inputs, the profile is treated as a stationary random process over the altitude interval of interest.

Equations of Motion

Response in the elastic modes of the vehicle can be expressed as

$$y(x,t) = a_1(t)\phi_1(x) + a_2(t)\phi_2(x) + \cdots \tag{21}$$

where $y(x,t)$ is the total bending deflection at a station x at time t; $a_n(t)$ is the contribution of mode n to the response at a reference station on the body; and $\phi_n(x)$ is the normalized shape of the nth natural mode. The coefficients a_n satisfy the following set of differential equations:

$$\ddot{a}_n + 2\zeta_n\omega_n\dot{a}_n + \omega_n^2 a_n = \frac{v_w(t)P_n}{M_n} \tag{22}$$

where for each mode n

M_n generalized mass, $\int_0^L m(x)\phi_n^2(x)dx$

ω_n natural vibration frequency of the mode

ζ_n equivalent viscous damping of the structure relative to critical damping

P_n generalized force per unit $v_w(t)$ due to an aerodynamic load distribution $p(x)$ along the vehicle (aerodynamic damping and stiffness effects have been neglected), $\int_0^L p(x)\phi_n(x)dx$

It is again convenient to express time in terms of the vertical distance traveled. Thus with

$$t = \frac{z}{V_Z} \tag{23}$$

where V_Z is the average velocity of the vehicle over the time interval of interest, equation (22) becomes

$$a_n'' + 2\zeta_n\Omega_n a_n' + \Omega_n^2 a_n = \frac{P_n}{V_Z^2 M_n} v_w(z) \tag{24}$$

where $\Omega_n = \omega_n / V_Z$ is the natural frequency in radians per unit length of distance traveled. It can be seen that the response in each mode is that of a damped spring-mass oscillator excited by a forcing function $v_w(z)$.

If instead of using the true profile $v_w(z)$ as a forcing function, the profile $v_b(z)$ measured by a wind sensor is applied, the differences in vehicle response in the two cases will represent the errors due to smoothing effects. The problem can be illustrated by the transfer-function block diagrams shown in figure 6. As indicated in the figure, the horizontal velocity of the wind

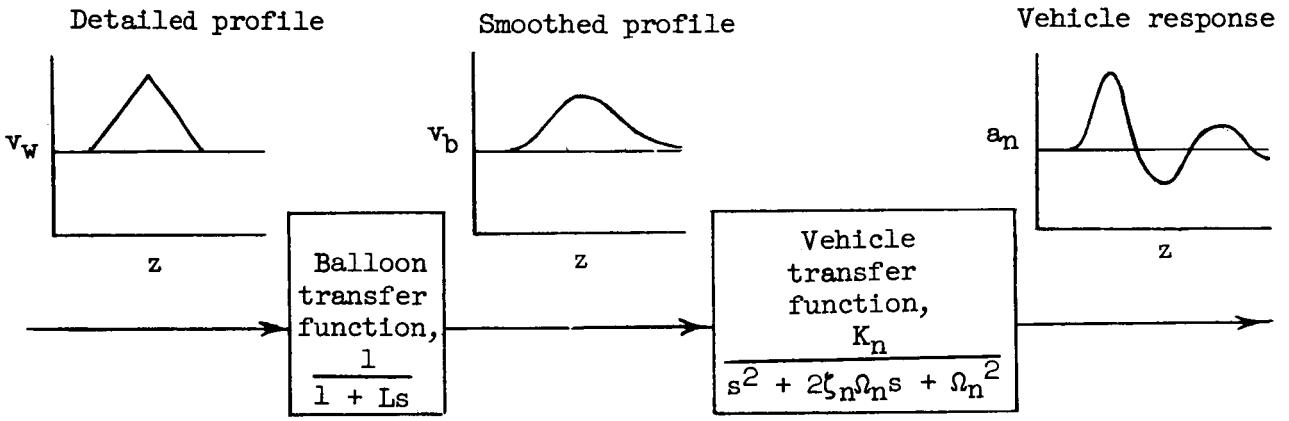

Figure 6.- Block diagram showing vehicle response to a balloon-measured wind profile.

sensor $v_b(z)$ is related to the wind profile $v_w(z)$ through the transfer function obtained by taking the Laplace transform of equation (10):

$$\frac{v_b(s)}{v_w(s)} = \frac{1}{1 + Ls} \tag{25}$$

The response of the vehicle is in turn related to the measured wind input through the transfer function obtained by taking the Laplace transform of equation (24) and substituting v_b for v_w:

$$\frac{a_n(s)}{v_b(s)} = \frac{K_n}{s^2 + 2\zeta_n\Omega_n s + \Omega_n{}^2} \tag{26}$$

where s is the Laplace operator and

$$K_n = \frac{P_n}{V_Z{}^2 M_n} \tag{27}$$

Thus, the vehicle response and the unfiltered wind profile are related as follows:

$$\frac{a_n(s)}{v_w(s)} = \frac{a_n(s)}{v_b(s)} \frac{v_b(s)}{v_w(s)} = \frac{K_n}{(1 + Ls)\left(s^2 + 2\zeta_n\Omega_n s + \Omega_n{}^2\right)} \tag{28}$$

By way of illustration, the response errors associated with the filtering properties of the wind sensor are considered next for two specific assumed forms of the wind profile - a discrete gust and a stationary random process.

Vehicle Response to a Discrete Gust

Assume the shape of $v_w(z)$ to be an isosceles triangle having a peak velocity of $v_{w,max}$ and an altitude increment b, "tuned" to give maximum dynamic amplification in the natural mode of interest; this occurs when the gust duration is approximately 0.8 times the wave length of the mode in question (ref. 12):

$$b = 0.8 \frac{2\pi}{\Omega_n} \tag{29}$$

From the inverse Laplace transform of equation (25), the velocity response of the wind sensor to the triangular gust under consideration is plotted in figure 7 for various values of the ratio L/b. Note that for $L/b = 0$ the sensor velocity and the input velocity are identical, whereas at $L/b = 0.2$ the indicated peak velocity is approximately three-fourths that of the input peak velocity.

The transient response of the vehicle to these "measured" gust profiles was obtained from solutions of equation (28) and is shown in figure 8. A condition of zero damping $(\zeta_n = 0)$ was assumed in the calculations. Also, for convenience, the response time histories are normalized with respect to the static response $(a_{st} = K_n/\Omega_n{}^2)$ and the distance traveled is expressed in gust lengths.

The point of chief interest in figure 8 is the reduction in the calculated maximum response of the vehicle which comes from using a filtered wind input. Therefore, in figure 9 the maximum response, as a fraction of the unfiltered maximum, is shown plotted against L/b. An alternate and perhaps more significant nondimensional parameter which is related to L/b through equation (29) can be written

$$\frac{\omega_n L}{V_Z} = 1.6\pi \frac{L}{b} \tag{30}$$

This parameter is also indicated on the abcissa of the figure. Note that $\omega_n L/V_Z$ uniquely relates the response errors due to smoothing to the three key variables of the problem, which are: L, the lag distance of the wind sensor; ω_n, the natural frequency of the vehicle; and V_Z, the velocity of the vehicle.

Vehicle Response to a Continuous Random Wind Input

Assume that the fine-grain structure of a wind profile can be represented as a stationary random process having a power spectrum $\Phi_{V_w}(\Omega)$. The power

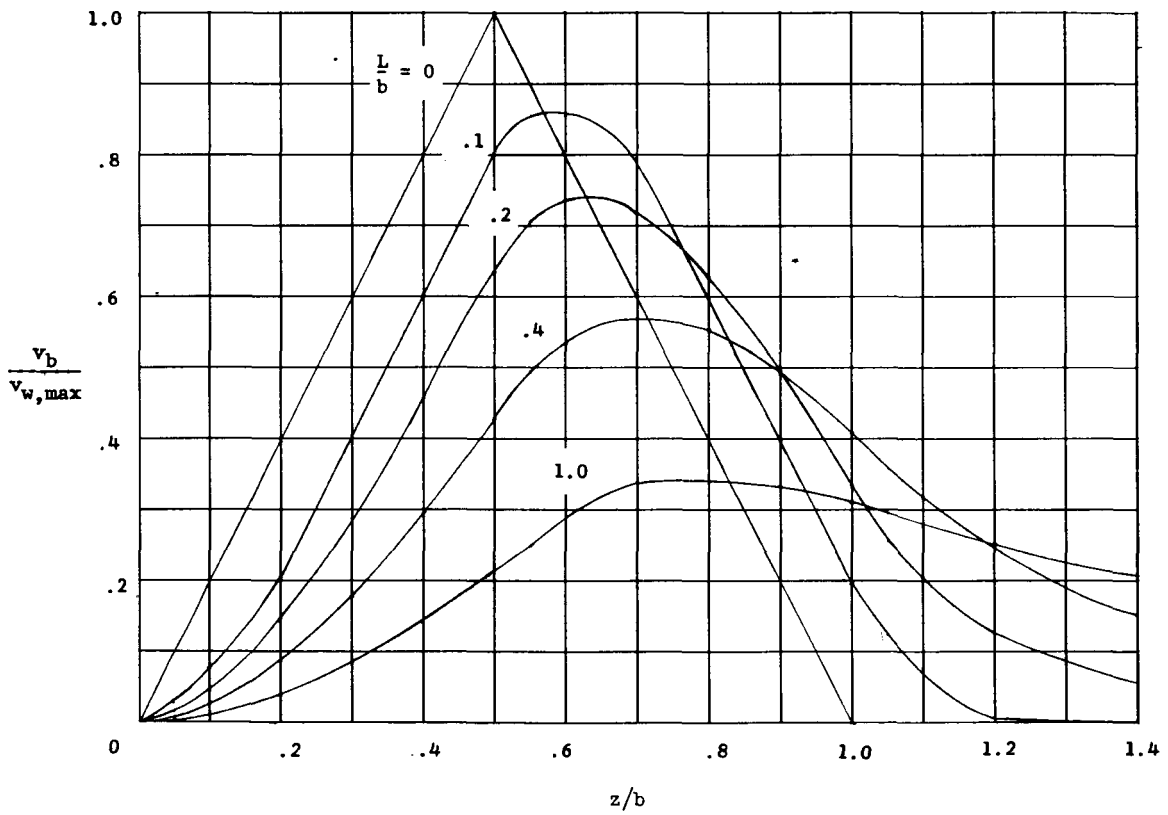

Figure 7.- Balloon response to triangular-shaped discrete gust.

spectrum of the vehicle response in the nth elastic mode is related to the power spectrum of the wind profile as follows:

$$\Phi_{a_n}(\Omega) = \left|H_V(\Omega)\right|^2 \Phi_{V_w}(\Omega) \tag{31}$$

where $H_V(\Omega)$ is the vehicle frequency-response function which can be derived from the Laplace transform of equation (24) by the substitution of $s = i\Omega$. Now

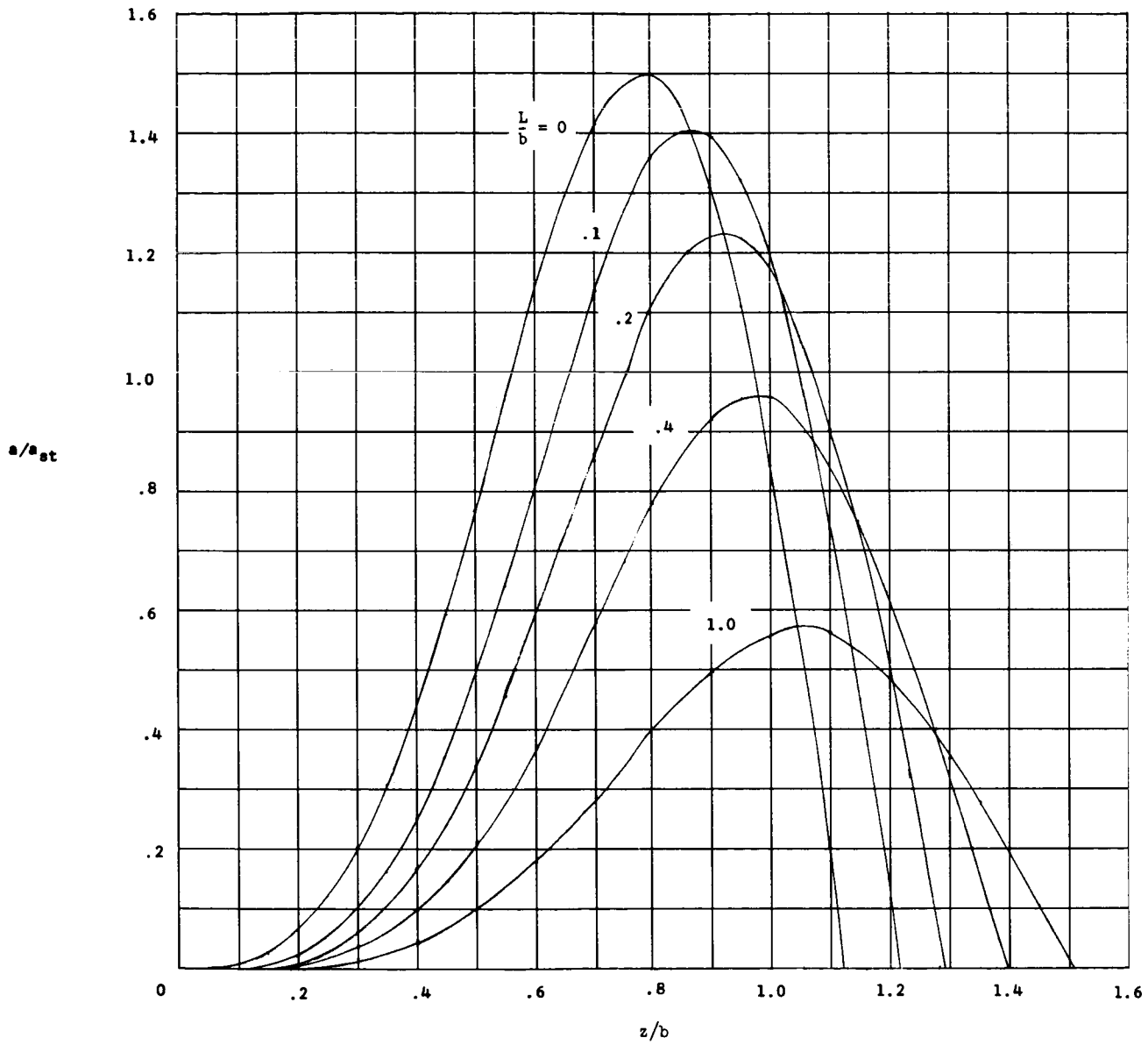

Figure 8.- Vehicle elastic-mode response to the "measured" gust in figure 7.

instead of the true wind profile as an input, consider the input as being a balloon-smoothed profile. The power spectrum of the smoothed profile is

$$\Phi_{V_b}(\Omega) = \left|H_b(\Omega)\right|^2 \Phi_{V_W}(\Omega) \tag{32}$$

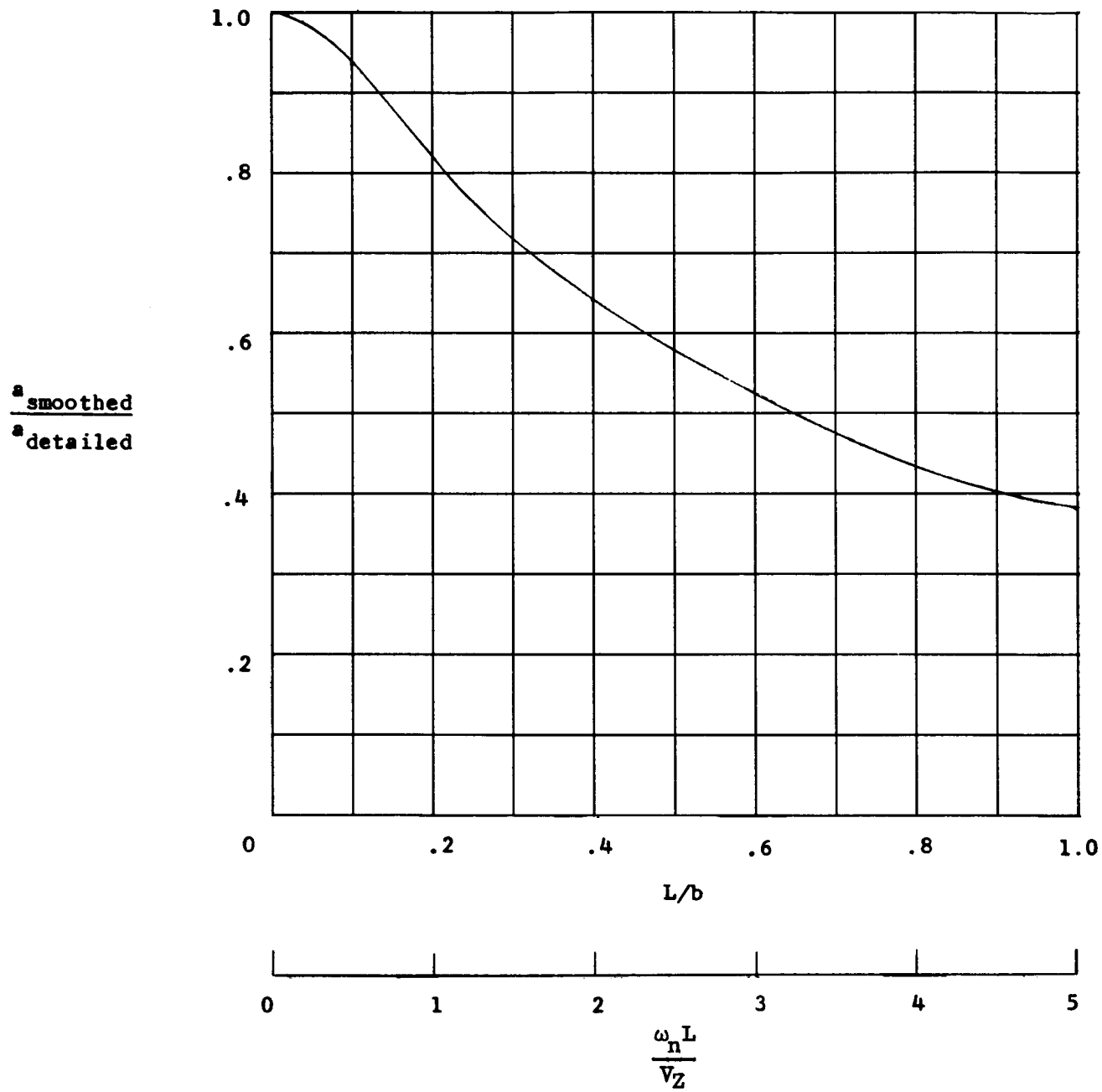

Figure 9.- Effects of balloon smoothing on the maximum elastic-mode response of a vehicle to a balloon-measured discrete gust input.

where $H_b(\Omega)$, the frequency response of the wind sensor, comes from equation (25) with $s = i\Omega$. Hence, the power spectrum of an elastic-mode response to a smoothed wind profile becomes

$$\Phi_{a_n}(\Omega) = \left|H_v(\Omega)\right|^2 \left|H_b(\Omega)\right|^2 \Phi_{v_w}(\Omega) \tag{33}$$

The mean square of the response is related to the power spectrum of the response by the expression

$$\overline{a_n^2} = \int_0^\infty \Phi_{a_n}(\Omega)d\Omega$$

$$= \int_0^\infty \left|H_v(\Omega)\right|^2 \left|H_b(\Omega)\right|^2 \Phi_{v_w}(\Omega)d\Omega \tag{34}$$

The elastic modes of a launch vehicle, being lightly damped, have frequency-response functions which are sharply peaked in the vicinity of the natural frequencies. Thus, for a random input whose frequency content is distributed in a continuous gradually changing manner, the response is governed primarily by the level of the input at the natural frequency of the mode in question. The mean-square response based on a smoothed input profile (eq. (34)) can therefore be written approximately as

$$\overline{a_n^2} \approx \left|H_b(\Omega_n)\right|^2 \Phi_{v_w}(\Omega_n) \int_0^\infty \left|H_v(\Omega)\right|^2 d\Omega \tag{35}$$

wherein it can be seen that the functions $H_b(\Omega_n)$ and $\Phi_{v_w}(\Omega_n)$ have been evaluated at the natural frequency Ω_n and removed from under the integral sign. Since the mean-square response based on an unsmoothed profile is obtained by letting L equal 0 in equation (35) to give $H_b(0) = 1.0$, the ratio of the smoothed to the unsmoothed mean-square response becomes

$$\frac{\left(\overline{a_n^2}\right)_{\text{smoothed}}}{\left(\overline{a_n^2}\right)_{\text{detailed}}} = \left|H_b\left(\frac{\omega_n L}{V_Z}\right)\right|^2 \tag{36}$$

or in terms of root-mean-square response, the ratio is simply the amplitude of the frequency-response function for the sensor:

$$\frac{\left(\sqrt{\overline{a_n^2}}\right)_{\text{smoothed}}}{\left(\sqrt{\overline{a_n^2}}\right)_{\text{detailed}}} = \left|H_s\left(\frac{\omega_n L}{V_Z}\right)\right| \tag{37}$$

This ratio, plotted in figure 10, represents the factor by which the predicted root-mean-square response would be attenuated by use of the balloon-smoothed profile in place of the detailed profile as an input. A comparison of the response-attenuation factors given by figure 9 for the triangular gust and by figure 10 for the continuous random profile indicates that smoothing effects are more pronounced for the case of random inputs.

As a specific example, wind profiles measured with the 2-meter spherical balloon of reference 6 will be used as the input in an evaluation of the response attenuation factors for a launch vehicle. Assume that at an altitude of 25,000 feet the vehicle has a vertical velocity V_Z of 1,000 feet per second and a fundamental natural bending frequency ω of 30 radians per second. With

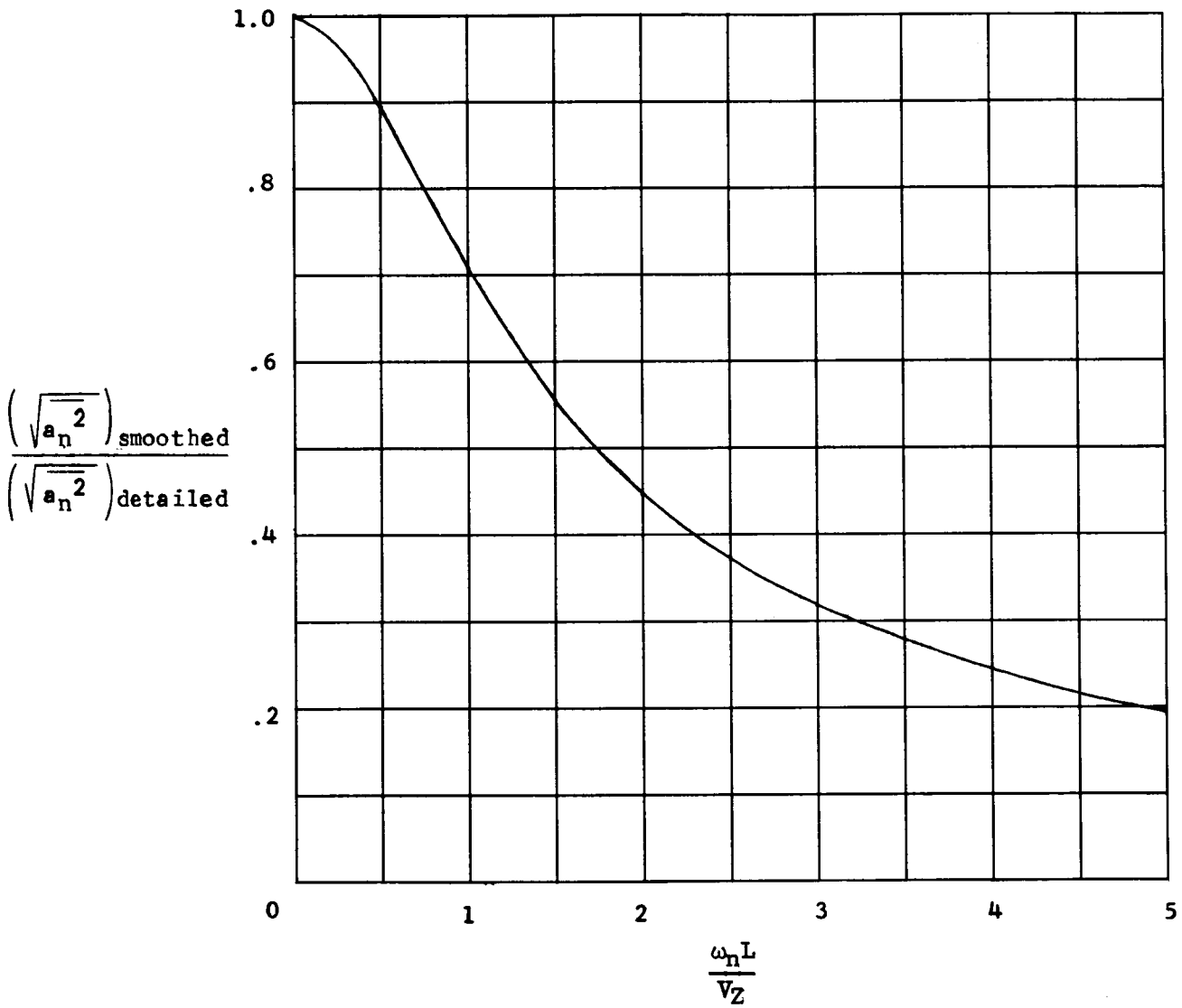

Figure 10.- Effects of balloon smoothing on the root-mean-square elastic-mode response of a vehicle to a balloon-measured continuous random wind input.

a balloon lag distance of 15 feet at this altitude (see table I) the nondimensional frequency parameter becomes $\frac{L\omega}{V_Z} = 15 \times \frac{30}{1,000} = 0.45$. Thus, the response attenuation due to balloon inertia is found to be 0.95 for the case of a "tuned" triangular gust (fig. 9) as compared with 0.91 for the random wind input (fig. 10).

CONCLUDING REMARKS

An analytical evaluation is made of the capabilities of balloon wind sensors to respond to the detailed variations in the wind structure which can represent important load inputs for flexible launch vehicles. Both rising and falling spherical balloons are considered. It is found that for a balloon of given weight there is an optimum diameter for which the balloon response velocity is most sensitive to variations in the profile of horizontal winds. When the diameter of the balloon is larger than this optimum value the advantages of reducing the balloon weight to improve its dynamic response become relatively insignificant. The apparent mass of ambient air surrounding the balloon, which has often been neglected in previous investigations, is found to be of considerable importance at lower altitudes where launch vehicles often encounter maximum aerodynamic loads.

An approximate "desmoothing" procedure is developed which, under certain conditions, can be used to correct measured wind profiles for smoothing errors associated with inertia of the balloon wind sensor. Finally, an assessment is made of the reduction in the calculated elastic mode response of launch vehicles that results when the fine-grain structure of a wind input is smoothed by balloon inertia. These errors are evaluated for continuous random and triangular-shaped discrete gust inputs.

Langley Research Center,
National Aeronautics and Space Administration,
Langley Station, Hampton, Va., April 18, 1963.

APPENDIX

RELATION BETWEEN LAG LENGTH OF A WIND SENSOR AND A RUNNING-AVERAGE LENGTH

Assume the wind profile $v_w(z)$ to be averaged over a distance that extends $l/2$ on each side of the altitude z. This running-average operation produces a smoothed profile defined as

$$\overline{v_w}(z) = \frac{1}{l} \int_{z-\frac{l}{2}}^{z+\frac{l}{2}} v_w(z)dz \tag{A1}$$

With an input $v_w(z)$ and an output $\overline{v_w}(z)$ a transfer function for the averaging operation can be determined from the ratio of the Laplace transforms of $\overline{v_w}(z)$ and $v_w(z)$. The Laplace transform of $\overline{v_w}(z)$ is

$$\overline{v_w}(s) = \int_0^\infty \overline{v_w}(z)e^{-sz}dz \tag{A2}$$

Introduction of a dummy variable of integration η and substitution of equation (A1) into equation (A2) gives

$$\overline{v_w}(s) = \frac{1}{l} \int_0^\infty \int_{\eta-\frac{l}{2}}^{\eta+\frac{l}{2}} v_w(\eta)e^{-sz}d\eta\, dz \tag{A3}$$

The integration of equation (A3) with respect to z produces

$$\overline{v_w}(s) = \frac{e^{\frac{sl}{2}} - e^{-\frac{sl}{2}}}{sl} \int_0^\infty v_w(\eta)e^{-s\eta}d\eta$$

$$= \frac{e^{\frac{sl}{2}} - e^{-\frac{sl}{2}}}{sl} v_w(s) \tag{A4}$$

Thus, the transfer function of the running-average operation becomes

$$\frac{\overline{v_w}(s)}{v_w(s)} = \frac{e^{\frac{sl}{2}} - e^{-\frac{sl}{2}}}{sl} \tag{A5}$$

With the substitution of $i\Omega$ for s in equation (A5), the frequency-response relation is obtained (also see appendix of ref. 13):

$$\frac{\overline{v_w}(\Omega)}{v_w(\Omega)} = \frac{\sin \frac{\Omega l}{2}}{\Omega l/2} \tag{A6}$$

Similarly, by substitution of $i\Omega$ for s in equation (25) the frequency-response amplitude function for the wind sensor is found to be

$$\left|\frac{v_b(\Omega)}{v_w(\Omega)}\right| = \frac{1}{\sqrt{1 + L^2\Omega^2}} \tag{A7}$$

Note that equations (A6) and (A7) are identical only at $l = 0$ and $L = 0$; however, an approximate equivalence between the l in equation (A6) and the L in equation (A7) can be established by expanding the two equations into a power series about $l = 0$ and $L = 0$ and equating the first-order terms of each expansion. Thus, a first-order approximation to equation (A6) is

$$\frac{\overline{v_w}}{v_w} \approx 1 - \frac{1}{24} l^2\Omega^2 \tag{A8}$$

and a first-order approximation to equation (A7) is

$$\left|\frac{v_b(\Omega)}{v_w(\Omega)}\right| \approx 1 - \frac{1}{2} L^2\Omega^2 \tag{A9}$$

Equating equations (A8) and (A9) gives the following relation between the running-average distance and the lag distance:

$$\begin{aligned} l &\approx \sqrt{12}L \\ &\approx 3.46L \end{aligned} \tag{A10}$$

REFERENCES

1. Sissenwine, Norman: Windspeed Profile, Windshear, and Gusts for Design of Guidance Systems for Vertical Rising Air Vehicles. Air Force Surveys in Geophysics No. 57 (AFCRC-TN-54-22), Air Force Cambridge Res. Center, Nov. 1954.

2. Henry, Robert M.: A Statistical Model for Synthetic Wind Profiles for Aerospace Vehicle Design and Launching Criteria. NASA TN D-1813, 1963.

3. Mazzola, Luciano L.: Design Criteria for Wind Induced Flight Loads on Large Boosted Vehicles. [Preprint] 2408-62, American Rocket Soc., Apr. 1962.

4. Scoggins, James R., and Vaughan, William W.: Cape Canaveral Wind and Shear Data (1 Thru 80 km) for Use in Vehicle Design and Performance Studies. NASA TN D-1274, 1962.

5. Henry, Robert M., Brandon, George W., Tolefson, Harold B., and Lanford, Wade E.: The Smoke-Trail Method for Obtaining Detailed Measurements of the Vertical Wind Profile for Application to Missile-Dynamic-Response Problems. NASA TN D-976, 1961.

6. Leviton, Robert: A Detailed Wind Profile Sounding Technique. Proceedings of the National Symposium on Winds for Aerospace Vehicle Design, Vol. 1. Air Force Surveys in Geophysics No. 140 (AFCRL-62-273(I)), Air Force Cambridge Res. Labs., Mar. 1962, pp. 187-195.

7. Scoggins, James R.: An Evaluation of Detail Wind Data as Measured by the FPS-16 Radar/Spherical Balloon Technique. NASA TN D-1572, 1963.

8. Morgan, Homer G., and Collins, Dennis F., Jr.: Some Applications of Detailed Wind Profile Data to Launch Vehicle Response Problems. AIAA Jour., vol. 1, no. 2, Feb. 1963, pp. 368-373.

9. Milne-Thomson, L. M.: Theoretical Hydrodynamics. Second ed., The Macmillian Co., 1950, pp. 415-416.

10. Lally, Vincent E., and Leviton, Robert: Accuracy of Wind Determination From the Track of a Falling Object. Air Force Surveys in Geophysics No. 93 (AFCRC-TN-58-213, ASTIA Doc. No. AD 146858), Air Force Cambridge Res. Center, Mar. 1958.

11. Leviton, Robert, and Wright, John B.: Accuracy of Density From the ROBIN Falling Sphere. GRD Res. Notes No. 73 (AFCRL 1095), Air Force Cambridge Res. Labs., Dec. 1961.

12. Jacobsen, Lydik S., and Ayre, Robert S.: Engineering Vibrations. McGraw-Hill Book Co., Inc., 1958.

13. Walls, James H., Houbolt, John C., and Press, Harry: Some Measurements and Power Spectra of Runway Roughness. NACA TN 3305, 1954.